Harasis, Salman; Mahmoud, Karar; Albatran, Saher; Alzaareer, Khaled; Salem, Qusay

Dynamic Performance Evaluation of Inverter Feeding a Weak Grid Considering Variable System Parameters

Published in:
IEEE Access

DOI:
10.1109/ACCESS.2021.3111047

Published: 07/09/2021

Document Version
Publisher's PDF, also known as Version of record

Please cite the original version:
Harasis, S., Mahmoud, K., Albatran, S., Alzaareer, K., & Salem, Q. (2021). Dynamic Performance Evaluation of Inverter Feeding a Weak Grid Considering Variable System Parameters. *IEEE Access*, *9*, 126104-126116. https://doi.org/10.1109/ACCESS.2021.3111047

IEEE Access
Multidisciplinary ⋮ Rapid Review ⋮ Open Access Journal

Received August 22, 2021, accepted September 5, 2021, date of publication September 7, 2021,
date of current version September 17, 2021.

Digital Object Identifier 10.1109/ACCESS.2021.3111047

Dynamic Performance Evaluation of Inverter Feeding a Weak Grid Considering Variable System Parameters

SALMAN HARASIS[1], (Member, IEEE), KARAR MAHMOUD[2,3], (Member, IEEE), SAHER ALBATRAN[4], (Senior Member, IEEE), KHALED ALZAAREER[5], (Member, IEEE), AND QUSAY SALEM[6], (Member, IEEE)

[1]Department of Electrical Power and Mechatronics Engineering, Tafila Technical University, Tafila 66110, Jordan
[2]Department of Electrical Engineering and Automation, Aalto University, 02150 Espoo, Finland
[3]Department of Electrical Engineering, Faculty of Engineering, Aswan University, Aswan 81542, Egypt
[4]Department of Electrical Engineering, Jordan University of Science and Technology, Irbid 22110, Jordan
[5]Department of Electrical Engineering, Faculty of Engineering, Philadelphia University, Amman 19392, Jordan
[6]Department of Electrical Engineering, Princess Sumaya University for Technology, Amman 11941, Jordan

Corresponding authors: Karar Mahmoud (karar.mostafa@aalto.fi) and Salman Harasis (salmanharasis@ttu.edu.jo)

ABSTRACT Interfacing a weak grid imposes challenges on distributed generators (DGs). These challenges include transient frequency and voltage dynamics that can destabilize the system. Accordingly, this paper investigates the grid stiffness based on different scenarios and the dynamics of a grid feeding DG connected to a weak grid. Moreover, the dynamic effects of the physical and control parameters on the system's stability are deeply analyzed and evaluated. Specifically, complete mathematical models and graphical representation are carried out to precisely examine the impact of the system parameters on the stability and performance of the DG. Therefore, stable deployment of renewable energy resources into power networks can be achieved as well as an efficient and robust performance of DGs can be ensured when connected to weak grids. The obtained results show the importance of the performed study in optimal sizing and designing the output filter of the inverter and the impact of tuning the control parameters on the system dynamics. As a result, a proper design of system physical and control parameters can be accurately achieved considering all factors affect the system performance. The paper also conducts detailed and elaborated analyses and simulations to evaluate the performance of a PI-controlled RC damped inverter connected to a weak grid. The proposed filter design of the interfacing inverter can significantly extend the integration of DGs into microgrids without requiring complex control schemes or oversized components.

INDEX TERMS Distributed generator, dynamic performance, frequency, stability, transient, weak grid.

I. INTRODUCTION

A weak grid usually describes a power network with a voltage distortion present at the point of connection (POC) [1]. The distortion occurs due to the highly inductive and resistive characteristics of the POC. The determination and classification of a grid stiffness are performed essentially based on the grid short circuit ratio (SCR) calculated using the grid impedance values. However, different indices have also been employed to describe and quantify the grid stiffness. Small grid impedance values result in a stiff grid with a high SCR. Large values of grid impedance seen at the POC result in a low SCR due to the increased voltage drop at the transmission lines [2]–[4]. This, in turn, deteriorates the voltage quality and the power transfer capability of the grid. Accordingly, the low SCR problem can be mitigated by connecting reactive power injectors; however, this solution increases the complexity and cost of the system [5], [6]. While the grid resistance impacts the magnitude of the POC voltage, a large variation in the grid inductance not only affects the voltage magnitude but also creates a phase shift that affects the active power flow at the POC. Moreover, increasing grid impedance value significantly affects the performance of the DG control that is

The associate editor coordinating the review of this manuscript and approving it for publication was Youngjin Kim.

tuned according to the known impedance value incorporated in the current control loop.

Practically, weak grid connection restricts active and reactive power injection. This restriction is also affected by the voltage stability limits of the system (which governs the flow of the reactive power) that is inversely proportional to the X/R ratio. The control of reactive power is associated with the characteristics of POC as reactive power injection depends on short-circuit capacity of the system, the equivalent impedance seen by the DG, and the type of the connected DG.

It is important to mention that both active and reactive power play essential roles in weak grid. The voltage profile in such weak connection is prone to instability under small disturbances where the voltage fluctuations are increased due to the enlarged transient energy transacted between the high grid impedance and the system components. The active power that is controlled through the phase angle of the voltage bus experiences severe dynamics when the phase swings due to the transient energy stored in the high impedance of the weak grid. In turn, the reactive power dynamics that affect the voltage magnitude and thereby voltage regulation of the connected bus are increased and exhibits poor management in weak grids. Furthermore, the natural coupling between the active and reactive power would affect both profiles under any disturbance due to their inherent interaction [6]–[8].

To improve the power quality of a grid-feeding DG, it is essential to know the real value of grid impedance. In many studies, the value of grid impedance is either fixed or estimated using different offline methods. Determining the grid impedance can be difficult since it is not constant and changes depending on the number of sources connected to the grid. To have a reliable control with a decent power quality profile, online determination of grid impedance in real-time can improve the performance of grid feeding DGs [9], [10].

Flexible ac transmission system (FACTS) devices can provide potential solutions for power quality and grid voltage-related issues especially in weak grid cases [5], [8]. In particular, to enhance the controllability of reactive power sharing and stabilize the grid voltage dynamics, different FACTS devices such as static Var compensator (SVC), unified power flow controller (UPFC), in addition to on-load tap changer mechanism are utilized to effectively regulate the reactive power sharing in a weak grid connection [5]. Among diverse FACTS variants, dynamic voltage restorers are the most prominent mechanisms used to alleviate power quality issues, that help maximizing the deployment of renewable DGs into power networks [7], [8].

Renewable DGs connected to weak grids have been studied in literature under different stiffness boundaries and aspects, especially in wind energy systems connected to high voltage networks [9]. Weak grids have been characterized for their low inertia [11], [12], low short circuit ratio [2], [3], high impedance value [9]–[12], and poor reactive power support [1], [2]. The existence of one or more criterion is enough to consider the grid as a weak grid. Therefore, attention needs to be paid when interfacing power electronic-based DGs that have complex controllers with a weak grid. DGs are sensitive to disturbances and the consequences of these disturbances have higher impacts on voltage and frequency stability profiles than conventional synchronous generators. Therefore, any load change or source switching may significantly affect system dynamics [17]. The sensitivity becomes of more concern when DGs are interfaced with weak grids. The voltage and frequency dynamics may lead to unstable operation if no proper control schemes and damping mechanisms are employed [17]–[19]. Efficient and high bandwidth controllers have to be designed to accommodate the dynamics and disturbances. Since the control actions depend on the system parameters, proper grid parameters' measurement is always required to ensure stabilized operation of the system under variable loading conditions and variable system configuration that influence impedance shape of the equivalent circuit. For these reasons, DGs require accurate controller tuning with sufficient bandwidth to ensure a stable grid-feeding source [20]–[23].

According to IEEE-1574 (interconnecting distributed resources with electric power systems standard) [24]–[26], the permissible frequency variation for grid-connected inverters is 1% for under-frequency and 0.8% for over-frequency deviations [26].

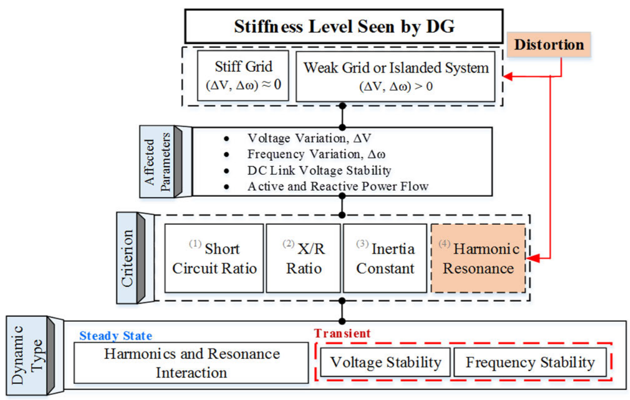

(1) [1, 2, and 11], (2) [9, 11, and 31], (3) [10, 14, and 15], (4) [26, 27]

FIGURE 1. Summary of stiffness criteria of POC.

The stiffness classification discussed in the literature does not have a unified definition in terms of the stiffness range. This is attributed to the different criteria and assumptions involved in analyzing the system from stability and controllers' design point of view. Parameters required to identify the stiffness of POC should be obtained to judge the stiffness level of the system. However, in most cases, it difficult to obtain the right values under all operating conditions. Fig. 1 shows an illustrative flowchart that includes the classification reported in the literature and helps to summarize several general aspects involved in investigating the stiffness level of the POC. The flowchart considers the primary criteria that affect the stiffness of the system and explains the associated dynamics in steady-state and transient operating modes.

The authors in [21] showed that the grid distortion increases the challenge of stabilizing the system even with small disturbance when the grid's inductive performance shifts the resonance frequency toward a lower frequency range. This is because the harmonic interactions induce the system instability and minimize the stability margins. Mitigating the impact of harmonic resonance interaction is associated with shifting the impedance intersection point to a higher possible frequency value where the harmonics have significantly low amplitudes. This point is found when the output impedance of the inverter ($\vec{Z}_{inv}$) equals the grid impedance ($\vec{Z}_g$) at the resonance frequency (ω_{res}). The work done in [27] showed that if the phase margin at the intersection point of a weak system is not large enough, the harmonic at this frequency will be amplified. Therefore, to ensure better resonance damping, the phase margin needs to be at least 30° (which is considered a high enough margin). The work reported in [28] showed that as the controller bandwidth is restricted for stability and noise purposes, one way to shift the resonance frequency is to employ an outer current loop with a multiple proportional resonance (PR) controller based on the predetermined resonance frequencies. This technique shapes the impedance of the output filter at the target frequencies through selective harmonic elimination. In [29], the authors proposed a proper optimal design for passive damping filter topology to mitigate the resonance problem that appears in the system. Many other works found in the literature characterized the weak-grid term by adding a relatively large inductance in series with the grid voltage in either renewable sources stability studies or in low voltage ride-through capability calculation for stability studies.

To cover the abovementioned research gap, this paper aims to extend the work done in the literature and investigates the effect of the system's physical and control parameters to obtain accurate modeling and efficient control design of grid-connected DG. Therefore, the dynamic performance of the system can be enhanced under significant disturbances, and the stability margins can be enlarged to tolerate larger disturbances. The majority of the work reported in the literature dealt with the weak grid challenge by designing complex controllers and nested control loops. In this work, the effect of physical circuit components and control parameters on the performance of (*i*) *active and reactive power-sharing profiles*, (*ii*) *voltage stability*, and (*iii*) *frequency stability* are investigated under different scenarios implementing a well-tuned PI-control. The dynamic performance of the system is examined under grid sag, variable grid impedance, and step-change in the connected load.

By studying and analyzing the system stability and performance under both steady-state and transient operating conditions, the contributions of the proposed work can be summarized as:

- Highlighting and characterizing the grid stiffness according to steady-state and transient criteria including harmonic distortion by investigating and analyzing all conditions that affect the stiffness including the harmonics.
- Investigating the effect of the system and controller parameters' change on system performance for (*i*) optimal tuning of control parameters, and (*ii*) optimal filter components sizing,
- Constructing a complete *transfer-function-based mathematical model*, and *block-diagram representation* to precisely examine and visualize the impact of the scheme's parameters on the stability and performance of grid-connected DG.
- Identifying the real and reactive control more precisely and provides a basis for stiffness identification, characterization, and classification.
- Showing the significant impact of filter impedance ($|Z_f|$) to grid impedance ratio (i.e., $|Z_f/Z_g|$) on the voltage and frequency stability.

The system considered in this study is shown in Fig. 2 where the inverter is fed from any renewable energy source and the output filter is an *RC*-damped filter. Practically, more than one generator can be connected to the grid even through parallel or distributed configurations. As the distributed lines affect the total impedance, the difference between these configurations is the equivalent impedance seen by the DG. In this work, we focus on a local solution to ensure stable deployment of each inverter-based renewable energy resource individually. Accordingly, the proposed solution can be used with multiple resources in a decentralized control scheme in which each resource works freely utilizing local measurements by the proposed solution.

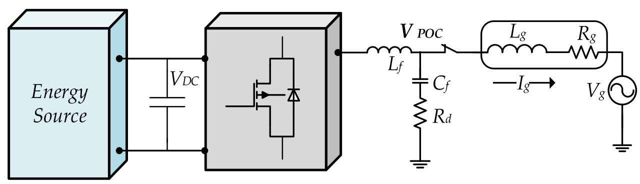

FIGURE 2. The equivalent circuit of grid feeding DG.

This paper is organized as follows: Section II presents the mathematical modeling of the DG interface to a high impedance grid and the active and reactive power equation depending on the coupling impedance. Section III evaluates the effect of grid stiffness on inverter stability by providing the complete modeling and block diagram representation. Section IV provides equivalent impedance determination and parameters effect analysis based on the modeling performed in section III. Section V shows the system modeling and dynamic simulation results. Section VI concludes the work carried out in the paper.

II. DG INTERFACE TO HIGH IMPEDANCE GRID

This part analyzes the effect of grid and inverter parameters on the system transient performance, including system modeling, grid analysis under different stiffness levels, and study the effect of parameter variation on voltage and frequency stability. Characterizing the grid stiffness should be considered for stable and efficient DG operation.

A. SCR RATIO CRITERION

The first aspect of identifying the grid connection is the SCR which represents the main criterion of grid stiffness. The higher the SCR, the stiffer the grid. A higher SCR value indicates larger currents delivered to the grid with an insignificant voltage drop. In other words, the phase shift between the current and the voltage of the POC is minimized so that the DG power delivered to the grid and the transmission efficiency can be maximized.

SCR can be quantified as a function of the grid equivalent circuit by the ratio of the short circuit power to the nominal power of the system (VA_{nom}) (i.e. per unit short circuit capacity) as given in (1).

$$SCR\left(R_g, X_g\right) = \frac{\left(V_g\right)^2 / |Z_g|}{VA_{nom}} = \frac{V_g^2}{VA_{nom}\left(\sqrt{R_g^2 + X_g^2}\right)} \quad (1)$$

where V_g and Z_g are grid voltage and impedance, respectively, R_g and X_g are the equivalent resistance and reactance of the grid impedance. Therefore, SCR value is inversely proportional to grid impedance. Several power system studies and standards, especially those of high voltage wind energy systems, consider a stiff grid with SCR equals to 10 or above and a weak grid for SCR less than 3 [14], [15], [30]–[32]. In a different research, an SCR equals to 3 or above is sufficient to consider the grid as strong considering the type of the connected inverter and the applied control [16]. Typically, DG connected to remote rural networks has very low SCR that endangers the voltage stability under any step change in the loadings or in generation [33], [34].

A smaller SCR value of the point where the DG is connected to the grid leads to several voltage issues. Voltage sag, swelling, spiking, and long-term distortion are among the most occurring issues in such systems with low SCR. These issues deteriorate the power quality of the system and impose extra challenges on the connected DG. At certain levels, voltage fluctuation induces voltage instability and causes undesirable system tripping.

B. X/R RATIO CRITERION

The second important aspect when DG is connected to the grid is X/R ratio. DG controllers can independently control the active and reactive power delivered to the grid. This can be efficiently achieved when the coupling between a DG and a grid is mostly inductive (i.e., the resistance is negligible). Based on the complex power delivered to the grid given in (2), the active and reactive power equations can be given as in (3) and (4), respectively.

$$S = VI^* = \frac{V_g V_{inv} \angle\theta - \delta}{|Z|} - \frac{V_g^2 \angle\theta}{Z} \quad (2)$$

$$P = \frac{V_g V_{inv}}{|Z|} cos\left(\theta - \delta\right) - \frac{V_g^2}{|Z|} cos\left(\theta\right) \quad (3)$$

$$Q = \frac{V_g V_{inv}}{|Z|} sin\left(\theta - \delta\right) - \frac{V_g^2}{|Z|} sin\left(\theta\right) \quad (4)$$

where δ is the voltage angle of the inverter considering the grid voltage angle is taken as a reference. Thus, (3) and (4) can be represented in their simplified forms as in (5.a) and (5.b).

$$P = \left[R\,cos\left(\delta\right) + X\,sin\left(\delta\right)\right] \frac{V_{inv} V_g}{R^2 + X^2} - \frac{V_g^2}{R^2 + X^2} R \quad (5.a)$$

$$Q = \left[X\,cos\left(\delta\right) - R\,sin\left(\delta\right)\right] \frac{V_{inv} V_g}{R^2 + X^2} - \frac{V_g^2}{R^2 + X^2} X \quad (5.b)$$

For the power coupling problem appears in (5), any change in active power command of the DG will dictate an undesired change in reactive power output and vice versa. This issue limits the power transfer capacity of the grid-connected system and impedes the control flexibility in achieving independent control of active and reactive power. Thus, this limitation imposes a new grid stiffness aspect that worsen the voltage, control, and power quality of the system. In real systems, higher X/R ratio of distribution lines yields a lower voltage regulation of the distribution feeder as seen in rural electrification. As a result, large voltage variation occurs and poor power quality, as well as, voltage stress problems appears. It is worthy to point out that, X/R ratio is also incorporated in SCR equation presented in (1), where the increased ratio X/R yields a poorer SCR value.

C. INERTIA CONSTANT (H) CRITERION

When a power converter interfaces a grid, the third stiffness criterion that appears during the transient is inertia. The voltage stiffness imposes frequency stiffness since both the magnitude and the phase of the voltage are affected during transients. The well-known swing equation describes this situation based on the inertia constant (H) [35]. The inverter-based DG as a non-inertial source is required to provide virtual inertia to support the frequency stability and improves the frequency profile. Virtual inertia sources and virtual synchronous machines have been proposed to enhance the frequency dynamics of DGs. The biggest challenge appears when a grid impedance increases and the inverter undergoes a transient event. The system experiences larger voltage and frequency oscillation during disturbances, which may quickly hit the stability boundaries. In this case, the dc-link voltage fluctuates significantly due to the disturbance and may become unstable [16], [36].

III. EVALUATING THE EFFECT OF GRID STIFFNESS ON INVERTER STABILITY

Interfacing DG to weak grids is of special concern, as the grid weakness imposes new challenges on inverter operation. Under weak-grid conditions, grid impedance variation will contaminate the voltage waveform by harmonics and augments the resonance, which in turn destabilizes the performance of the inverter and degrade the power quality. In particular, even though the grid harmonics affect the steady-state operation of the system, its impact on the transient is rather complex and severe. This is because the PLL control loop requires more time to chase the fundamental phase information and the error of its PI control converges to zero after several cycles. As a matter of fact, this delay time would drive the system into unstable operation mode if the harmonic contamination increases or a stronger disturbance occurs. As a result, harmonic existence would turn the power quality into power stability issues.

At the same time, any increase in the filter output inductance would augment the resonance problem and resonate with high grid equivalent inductance at a low-frequency range. Therefore, active damping or harmonic elimination control schemes should be adopted [37], [38].

The equivalent circuit of the grid-connected DG system is shown in Fig. 3, where the equivalent circuit of the grid shows the series grid impedance (L_g and R_g). The damped LC filter is optimized based on [29].

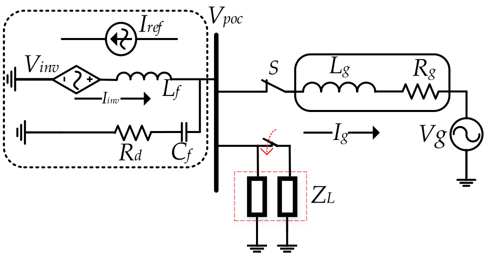

FIGURE 3. The equivalent circuit of the grid-connected DGs.

Generally, an *LCL* filter is high order filter that provides sufficient attenuation and stabilizes the inverter in grid-connected and islanded modes [72]. The LC filter considered in this work represents an LCL filter considering the equivalent inductance of the weak grid. However, the larger value of L_g in weak grid cases and the variation of its equivalence shifts the resonance frequency close to the fundamental frequency. Therefore, harmonics in the neighborhood of resonance frequency can be augmented and destabilize the system under small fault or disturbance. The resonance is a major steady-state issue that easily causes voltage collapse during transients. The resonance frequency as a function of grid inductance is given in (6) and depicted in Fig. 4.

$$f_{res} = \frac{1}{2\pi}\sqrt{\frac{L_f + L_g}{L_f L_g C_f}} \tag{6}$$

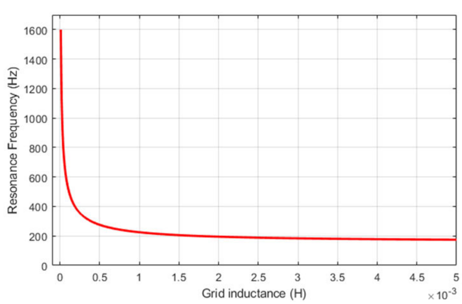

FIGURE 4. The resonance frequency as a function of Lg.

The transfer function can provide a way to study the dynamic interaction of the voltage and the current. It represents the equivalent admittance/impedance and can show the impact of change in system parameters on the stability of the system. The needed control action can be taken accordingly. The relations between the current and voltage of DG system in Fig. 3 considering $R_g = 0$ are shown as follows:

$$I_g = [V_{poc} - V_g]\frac{1}{sL_g} \tag{7}$$

$$I_{inv} = [V_{inv} - V_{poc}]\frac{1}{sL_f} \tag{8}$$

$$V_{poc} = V_{c_f} + V_{R_d} \tag{9}$$

$$V_{poc} = [I_{inv} - I_g]\frac{(1 + R_d C_f)}{sC_f} \tag{10}$$

A block diagram model that links the input inverter voltage with the current delivered to the grid is shown in Fig. 5, where the grid voltage is represented as a second input (disturbance).

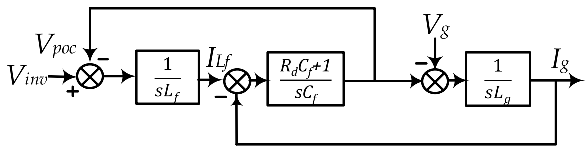

FIGURE 5. The block diagram of the system equivalent circuit.

To show the impact of the grid impedance on the system stability, the equation describes the relationship between the inverter output current (I_{Lf}) and equivalent voltage seen at POC, the admittance ($Y(s)$), is derived and given in (11). The equivalent voltage seen at POC is the disturbance ($D(s)$) multiplied by the grid voltage. $Y(s)$ is the transfer function between the inverter current and the grid voltage. This relation can be further simplified as shown in Fig. 6.

$$\begin{aligned} I_{L_f}(s) &= \left[\frac{s^2 C_f L_g + sC_f R_d + 1}{s^3 C_f L_g L_f + s^2\left(R_d C_f L_g + R_d C_f L_f\right) + s(L_f + L_g)}\right] \\ &\quad \times \left[V_{inv}(s) - \frac{sR_d C_f + 1}{s^2 C_f L_g + sC_f R_d + 1} V_g(s)\right] \\ &= Y(s)\,[V_{inv}(s) - D(s)V_g(s)] \end{aligned} \tag{11}$$

$$I_{Lf}(s) = \frac{K_{inv}\left(k_p s + k_i\right)}{s^2 L_f + K_{inv} k_p s + K_{inv} k_i} I_{Lf(ref)}(s) \tag{12}$$

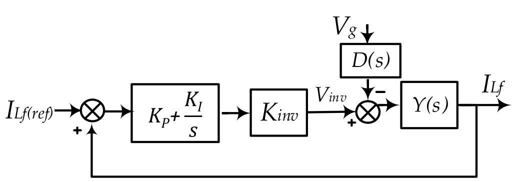

FIGURE 6. Block diagram of the closed-loop current control.

IV. EQUIVALENT IMPEDANCE DETERMINATION AND PARAMETERS EFFECT ANALYSIS

The inverter output impedance is affected not only by its output filter type but also by control loop gains [32]. Therefore, the gains of the current control loop shape the inverter impedance/admittance along with the frequency axis. The inverter's current given in (11) combines both inverter and grid admittance components. In order to determine the inverter output impedance, the block diagram of Fig. 5 is modified and redrawn as in Fig. 7 to segregate the two admittances. The dashed part of Fig. 7 is derived from the current control loop considering $Z_{inv}(s)$ as Thevenin's impedance of the inverter seen at POC. The inverter output current, I_{Lf}, can be expressed in terms of control and physical filter parameters, as shown in (12).

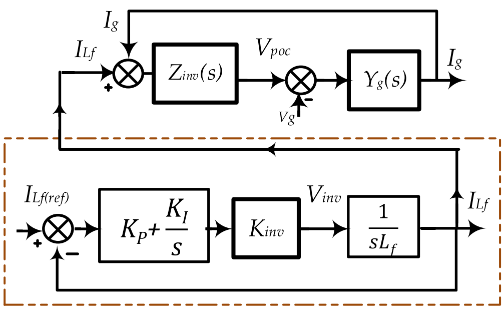

FIGURE 7. Block diagram representation of Eq. (11) including the control loop.

The transfer function of (12) shows that a second-order dynamic of the current control loop needs to work with a reasonable damping ratio for stable operation based on a well-tuned K_p and K_i, while K_{inv} is unity gain represents the PWM modulation gain [13], [39]. Fig. 7 shows the overall block diagram of the current controlled inverter grid-connected. To find the representation of $Z_{inv}(s)$ and referring to Fig. 8, the equivalent impedance is shown in Fig. 9, where the transfer function $Z_{inv}(s)$ can be obtained based on (13).

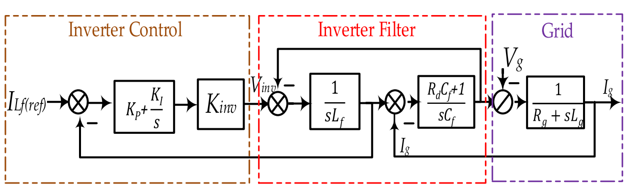

FIGURE 8. Overall block diagram of the system of current-controlled DG.

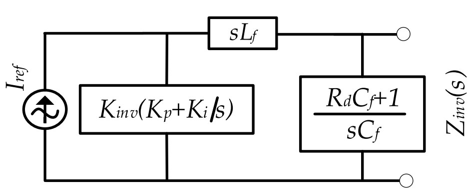

FIGURE 9. The inverter equivalent circuit for obtaining the equivalent impedance.

To design a well-performed current control loop, the speed of response, disturbance rejection, and stability margins are considered for optimal control parameter tuning. The quantity $K_{inv}, k_p, k_i/s$ given in (12) should be high enough for good reference current tracking. Moreover, the quantity $\left(\frac{sR_dC_f+1}{s^2C_fL_g+sC_fR_d+1}\right)$ given in (11), which has an uncontrolled parameter (L_g) should have a small impact on the step response of the transfer function for good grid disturbance rejection. Theoretically, this can be achieved if the denominator is much larger than the numerator that could approximately yield $\frac{1}{\infty}$ or negligible disturbance effect.

$$Z_{inv}(s) = \frac{\frac{R_dC_f+1}{sC_f}\left(sL_f + K_{inv}(k_p + k_i/s)\right)}{\frac{R_dC_f+1}{sC_f} + sL_f + K_{inv}(k_p + k_i/s)} \tag{13}$$

Fig. 10 shows the filter parameters' impact on the weak grid voltage response (disturbance rejection). The response shows that increasing the inverter output filter's capacitance reduces the voltage overshoot, and the damping resistor can significantly damp the oscillation.

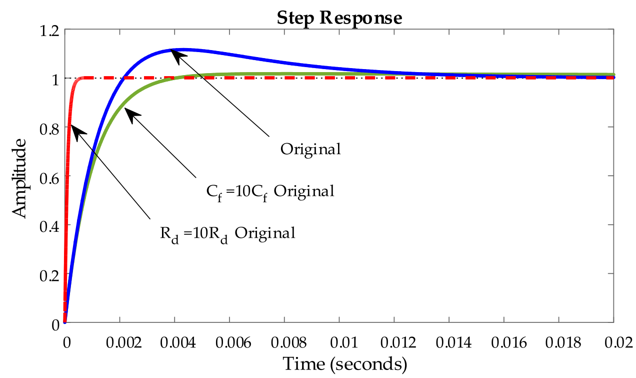

FIGURE 10. Step response of the grid disturbance part.

Equation (14), as shown at the bottom of the next page, summarizes the target when interfacing a weak grid where good current tracking and disturbance rejection can be achieved by optimizing the filter parameters and proper controller tuning. The tracking capability of the system under study is judged by observing the difference between the commanded current value of the grid feeding DG type with the measured current value. The dynamic difference between these values indicates the effectiveness level of system tracking capability and control bandwidth. Equation (14) in the manuscript explains the tracking of the system reference current.

The equation has two parts; in the tracking part, for good tracking, the numerator should have a large value in order to equalize the denominator and ignoring the effect of the constant 1 in the denominator. This can be achieved by having larger gains where $I_{Lf} \approx \frac{1}{1} I_{Lf(ref)}$. In the disturbance rejection part, for good disturbance rejection, the denominator should be much larger than the numerator. This would allow the second term of the equation to approach zero and

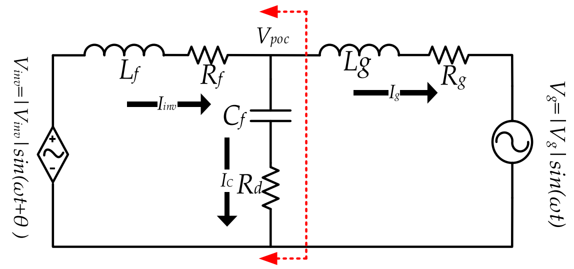

FIGURE 11. The equivalent circuit of the grid feeding DG.

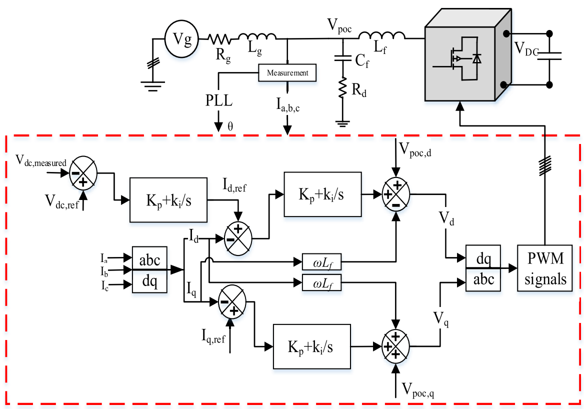

FIGURE 12. The configuration of DG grid feeding system.

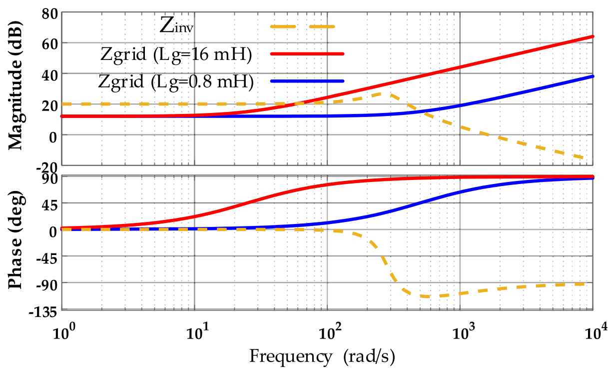

FIGURE 13. Resonance frequency comparison based on Z_g.

minimizes the effect of the disturbance. Increasing the proportional gain (k_p) leads to significantly increase the bandwidth of the control system by increasing the gain margin and thereby the damping of the system. This is because the proportional gain impacts the equivalent impedance shaping at high frequency. However, this may worsen the stability by introducing high-frequency noise to the system if no proper and optimized tuning of the gains is performed.

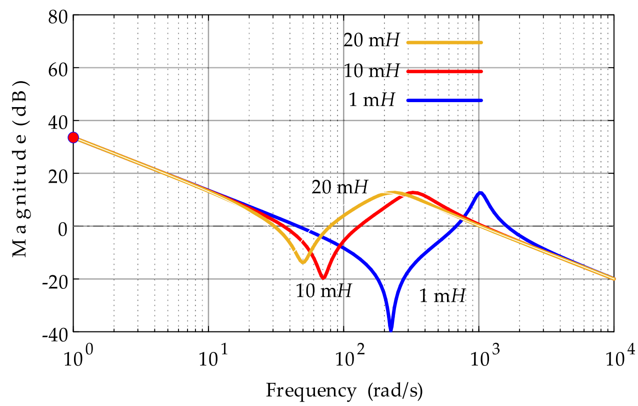

FIGURE 14. Y(s) shape when Lg changes from (1-20) mH.

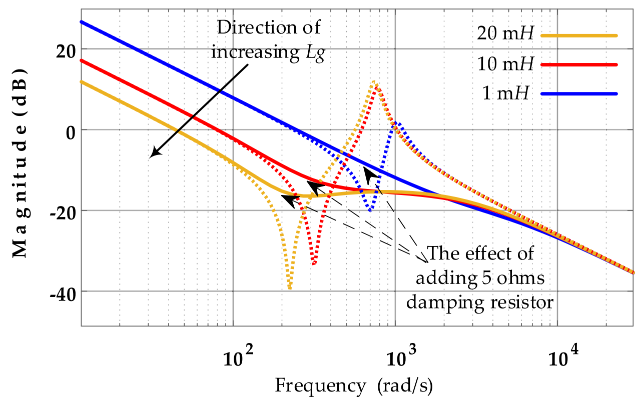

(a)Bode plot

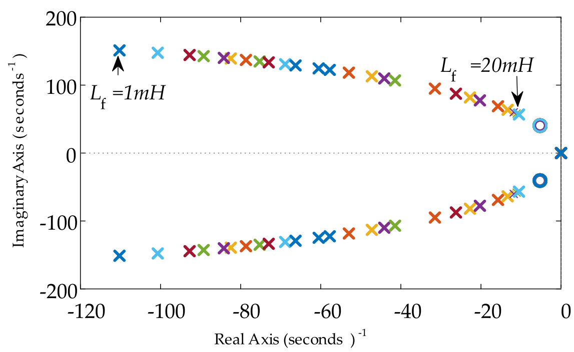

(b) Pole-zero mapping

FIGURE 15. The positive effect of increasing filter inductance L_f when the grid inductance (L_g = 20 mH).

To determine the X/R ratio, the grid connection's resistance is taken into account in calculating the equivalent grid impedance (Z_g). The resistor deteriorates the control due to the coupling between active and reactive power control [39].

$$I_{Lf}(s)=\frac{K_{inv}(k_p+k_i/s)Y(s)}{1+K_{inv}(k_p+k_i/s)Y(s)}I_{Lf(ref)}(s)+\frac{D(s)Y(s)}{1+K_{inv}(k_p+k_i/s)Y(s)}V_g(s) \tag{14}$$

$$K(s)=\left.\frac{V_{poc}(s)}{V_{inv}(s)}\right|_{V_g=0}=\frac{s^2(L_gR_dC_f)+s\left(L_g+C_fR_dR_g\right)+R_g}{s^3(L_fL_gC_f)+s^2\left[(L_fC_f\left(R_d+R_g\right)+L_gC_fR_d\right]+s\left[L_f+L_g+R_gC_f\left(R_d+1\right)\right]+R_g} \tag{15}$$

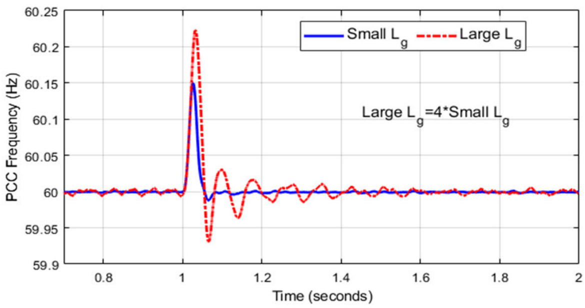

(a) The PCC frequency

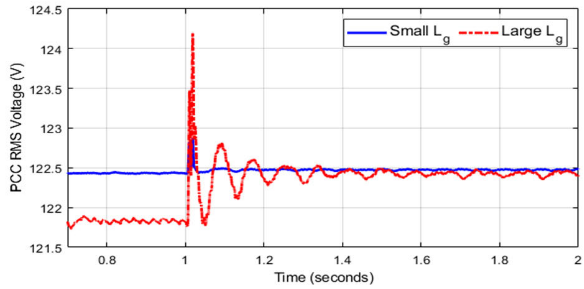

(b) The PCC voltage

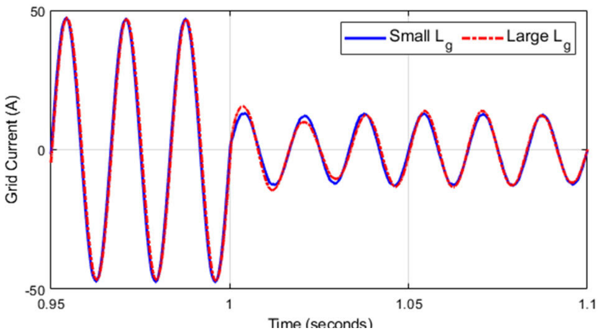

(c) The grid current

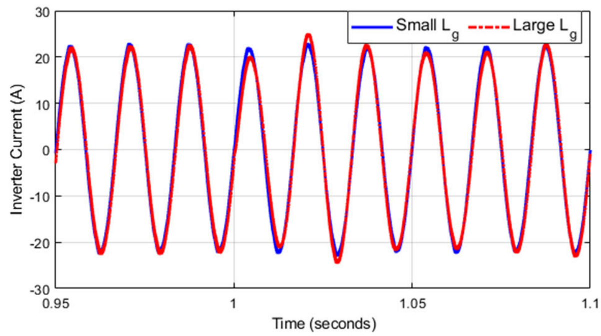

(d) The inverter current

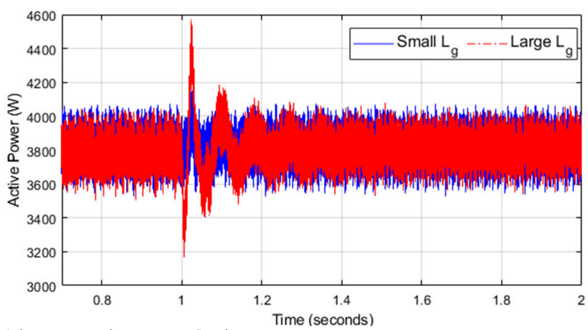

(e) inverter active power-sharing

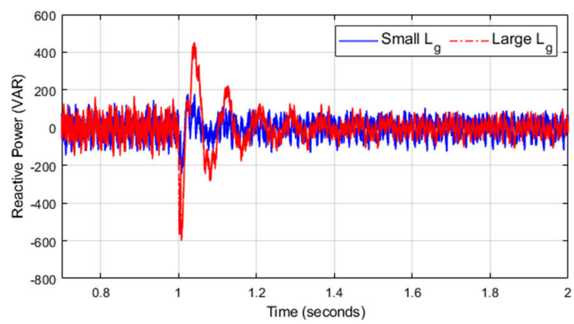

(f) inverter reactive power-sharing

FIGURE 16. System response to step load change under small (L_g = 0.5 mH) and large (L_g = 3 mH) grid inductance.

To determine the loop, transfer function which expresses the admittance of the equivalent circuit, the same procedure is performed. Knowing that the dynamic voltage gain, $K(s)$, is given in (15), as shown at the bottom of the previous page.

To find the equivalent admittance, $V_g(s)$ is set to be zero i.e., $Ig(s) = V_{poc}(s)/(sL_g + R_g)$ and the transfer function of the grid current and the inverter voltage can be written as in (16).

$$\left.\frac{I_g(s)}{V_{inv}(s)}\right|_{V_g=0} = \frac{K(s)}{(sL_g + R_g)} \tag{16}$$

V. RESULTS AND CASE STUDIES

The system shown in Fig. 12 has been simulated in Matlab/ Simulink. The parameters of the system are given in Table 1. Fig. 13 shows the problem of low-frequency resonance where high grid inductance shifts the impedance intersection point (Z_g/Z_{inv}) around ten times to the lower frequency range. This, in turn, augments the system stability problem and increases the probability of instability occurrence under smaller system dynamics.

The adverse effect of increasing L_g on the admittance shape and how the filter damping resistor (R_d) can mitigate its effect is shown in Fig. 14. It is important to show how larger

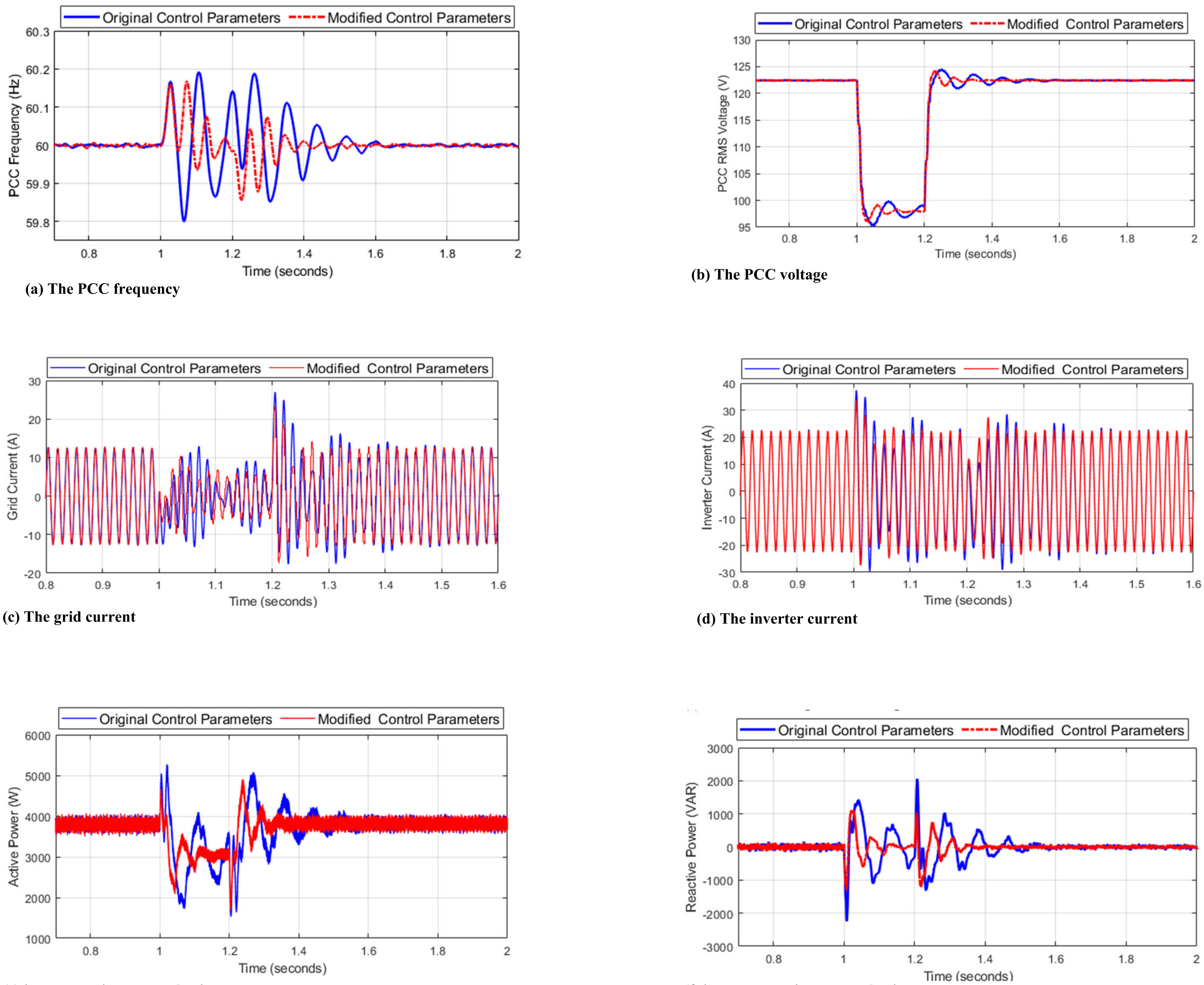

(a) The PCC frequency

(b) The PCC voltage

(c) The grid current

(d) The inverter current

(e) inverter active power sharing

(f) inverter reactive power sharing

FIGURE 17. The waveforms of the system measured value under voltage sag when the output filter parameters are changed ($K_i = 0.3 \rightarrow 0.9$, $K_p = 1400 \rightarrow 3000$).

inverter output inductance helps in mitigating the effect of low stiffness levels.

Fig. 15 shows an increase in L_f, which in turn reduces the impact of the grid weakness, Fig. 15(a) shows the magnitude plots of different L_f values. Fig. 15(b) shows the root mapping of the system and how increasing the filter impedance reduces the damping but shift the resonance to a lower frequency range which means increasing L_f only is not enough to stabilize the system effectively and the control part should take a role in the damping.

Different cases have been considered to evaluate the change in system parameters on the output waveforms. Fig. 16 (a) through Fig. 16 (f) compare the waveforms of the system measured value when a step load change occurs under small (L_g = 0.5 mH) and large (L_g = 3 mH) grid inductance cases. The results show that the frequency and voltage dynamics are considerably affected due to the increase in grid inductance. Further, the active and reactive power sharing undergoes a large transient deviation due to the large grid inductance.

TABLE 1. System parameters.

Parameter	Symbol	Value
DC link voltage	V_{dc}	400 V
DC link capacitor	C_{dc}	5.6 mF
Damping resistor	R_d	1-2.21 ohm
Filter capacitance	C_f	1mF
Filter inductor	L_f	1.9 mH
switching frequency	f_{sw}	20 kHz
Grid inductance	L_g	0.2 uH-4.14 mH
Grid resistance	R_g	1ohm
Rated frequency	f	60 Hz
Rated line voltage	V	208 V
DG rating	VA	7 kVA
X/R ratio (L_g=0.2 uH - 4.14 mH)	-	≈0.075−1.7
SCR ratio (L_g=0.2 uH - 4.14 mH)	-	≈43-1.3

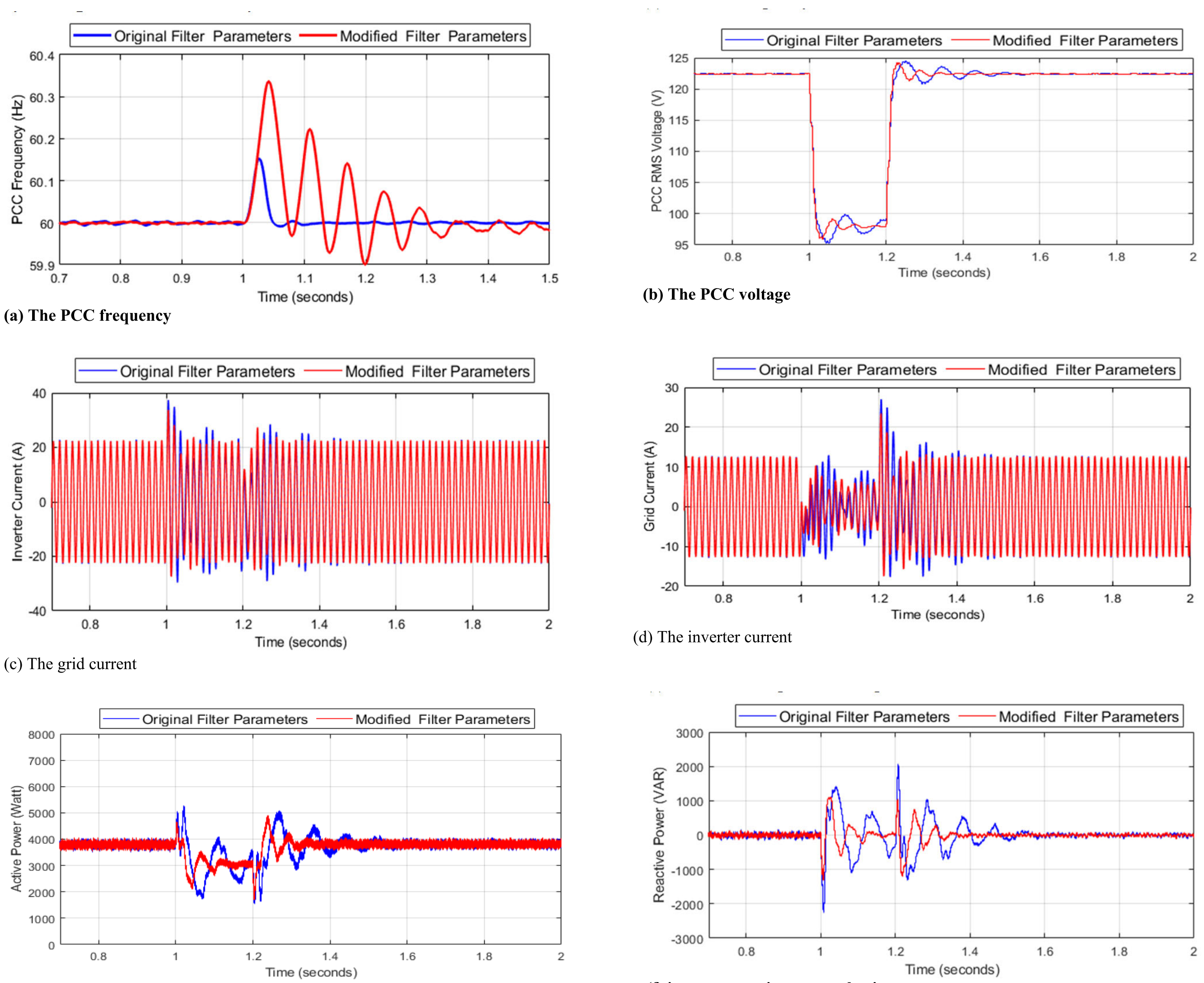

(a) The PCC frequency

(b) The PCC voltage

(c) The grid current

(d) The inverter current

(e) inverter active power sharing

(f) inverter reactive power sharing

FIGURE 18. The waveforms of the system measured value under voltage sag when the output filter parameters are changed (C_f = 1mF → 3mF) and (R_d = 0.5 → 10Ω).

Under weak grid connection, three cases have been considered where a voltage sag has been introduced to evaluate the effect of the change in control parameters (case-1), filter parameters (case-2), and damping (case-3) on the system measured value.

Case-1: The values of K_i and K_p of the inner current loop have been changed from 0.3 to 0.9 and from1400 to 3000, respectively. A 20% voltage sag is introduced for 2 seconds to examine the system response under sudden voltage variation. The results are shown in Fig. 17(a) through Fig. 17(f). The results show that under the original control gains, the tracking during steady-state is sufficient. However, during the sag period, the system exhibits more oscillations and deviations due to the limited bandwidth. On the other side, the increased gains help the system to quickly minimize the error and show better tracking due to the larger bandwidth.

Case-2: The values of C_f and R_d of the output filter shunt branch have been changed from 1 mF to 3 mF and from 0.5Ω to10 Ω, respectively. A 20% voltage sag is introduced for 2 seconds to examine the system response under sudden voltage variation. The results are shown in Fig. 18(a) through Fig. 18(f). It can be seen from the results that increasing the shunt capacitor decreases the natural frequency (See Eq. (6)). Therefore, the system damping and stability can be enhanced.

Compared to the result shown in Fig. 17 and referring to Eq. (14) and Eq. (15), it can be concluded that sizing the physical parameters and tuning the controller gains play a significant role in stabilizing the system. However, increasing the controller gains at the expense of the size of the physical parameter leads to introducing switching frequency noise and resonance. This, in turn, makes the system prone to instability.

Case-3: In order to observe the effect of the damping on the performance of the LC filter, the system has been operated under different damping resistance values. A 20% voltage sag is introduced for 2 seconds to examine the system response under sudden voltage variation. The results are

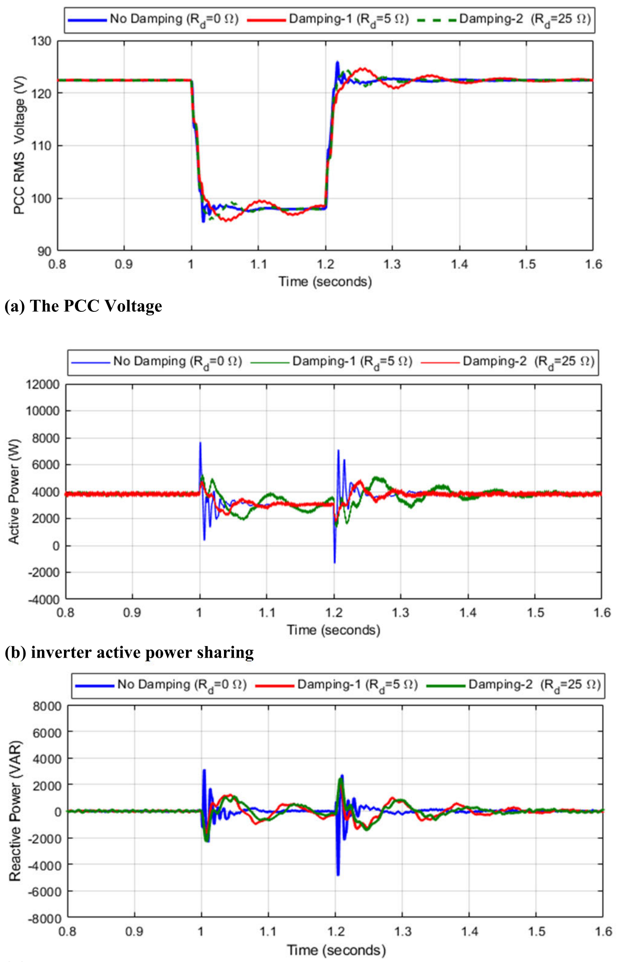

(a) The PCC Voltage

(b) inverter active power sharing

(c) The inverter reactive power-sharing

FIGURE 19. The waveforms of the system voltage and power-sharing profiles under voltage sag when the damping is changed (Rd = 0 → 25Ω).

shown in Fig. 19(a) through Fig. 18(c). It can be seen from the results that the damping resistor is important to damp the peak power oscillations that cause protection relay tripping as the peak power hits kW and kVar ranges. Furthermore, increasing the damping resistor from 0 to 25 Ω agrees with the modelling results shown in Fig. 10. Moreover, the damping rejects the voltage disturbance and reduces the voltage ringing and overshoot that may severely hurt the inverter switches.

VI. CONCLUSION

This work deals with evaluating the dynamic performance of distributed energy resources connected to a weak grid. Stiffness classifications of the point of connection, including the mathematical formulation, are carried out to establish a clear background about weak grid applications. Thorough evaluations have been performed to examine all the factors that affect the performance of distributed generators. Through complete modeling of the system and frequency domain analyses, this work reveals the impact of the control and physical parameters on the tracking capability and disturbance rejection of the model on system dynamics. After that, time-domain simulations have been performed to validate the findings and prove the paper's modeling. It was found that the grid impedance deteriorates the system stability and augments the low-frequency resonance problem. Furthermore, the results show the impact of the equivalent impedance on the frequency profile and how the proper filter design of the inverter can strengthen the system stability and increase the stability margins by shaping the equivalent impedance. As a result, increasing the integration of DGs into microgrids can be effectively extended without the need for complex control strategies or oversized DG components. Compared to the work reported in [38] which implements a robust H_∞ cascaded control strategy, this paper demonstrates that under well designed system and control parameters, simple PI control is able to work under sufficient bandwidth that provides satisfied tracking capability and rejects the grid voltage disturbances.

The complexity of the proposed control arises from the complete knowledge of the grid parameters which is difficult most of the time. As the equivalent impedance seen by the connected DG is affected by the number and the location of the other DGs connected to the grid, continuous measurement and estimation of the equivalent impedance is required. This, in turn, complicates the full controllability of grid feeding DG. Developing identification and estimation methodologies helps to accurately identify the values of the grid equivalents seen at the POC under all operating and loading conditions. Currently, the authors are working on this.

REFERENCES

[1] B. Arif, L. Tarisciotti, P. Zanchetta, and J. Clare, "Finite set model predictive control with a novel online grid inductance estimation technique," in *Proc. 7th IET Int. Conf. Power Electron., Mach. Drives (PEMD)*, 2014, pp. 1–6.

[2] B. Arif, L. Tarisciotti, P. Zanchetta, J. C. Clare, and M. Degano, "Grid parameter estimation using model predictive direct power control," *IEEE Trans. Ind. Appl.*, vol. 51, no. 6, pp. 4614–4622, Nov./Dec. 2015.

[3] J. Xu, S. Xie, and T. Tang, "Evaluations of current control in weak grid case for grid-connected LCL-filtered inverter," *IET Power Electron.*, vol. 6, no. 2, pp. 227–234, Feb. 2013.

[4] L. Yang, X. He, P. Zhang, and S. Liu, "Control scheme and performance analysis of dual-frequency single-phase grid-connected inverter interfaced with weak and distorted grids," *IEEE Access*, vol. 8, pp. 178639–178650, 2020.

[5] A. K. Pathak, M. P. Sharma, and M. Bundele, "A critical review of voltage and reactive power management of wind farms," *Renew. Sustain. Energy Rev.*, vol. 51, pp. 460–471, Nov. 2015.

[6] S. M. Alizadeh, C. Ozansoy, and T. Alpcan, "The impact of X/R ratio on voltage stability in a distribution network penetrated by wind farms," in *Proc. Australas. Universities Power Eng. Conf. (AUPEC)*, Sep. 2016, pp. 1–6, doi: 10.1109/AUPEC.2016.7749289.

[7] D. Kim, H. Cho, B. Park, and B. Lee, "Evaluating influence of inverter-based resources on system strength considering inverter interaction level," *Sustainability*, vol. 12, no. 8, p. 3469, 2020, doi: 10.3390/su12083469.

[8] G. S. Chawda, A. G. Shaik, O. P. Mahela, S. Padmanaban, and J. B. Holm-Nielsen, "Comprehensive review of distributed facts control algorithms for power quality enhancement in utility grid with renewable energy penetration," *IEEE Access*, vol. 8, pp. 107614–107634, 2020, doi: 10.1109/ACCESS.2020.3000931.

[9] N. Hoffmann and F. W. Fuchs, "Minimal invasive equivalent grid impedance estimation in inductive–resistive power networks using extended Kalman filter," *IEEE Trans. Power Electron.*, vol. 29, no. 2, pp. 631–641, Feb. 2014.

[10] Z. Xie, Y. Chen, W. Wu, Y. Xu, H. Wang, J. Guo, and A. Luo, ''Modeling and control parameters design for grid-connected inverter system considering the effect of PLL and grid impedance,'' *IEEE Access*, vol. 8, pp. 40474–40484, 2020.

[11] Y. Sun, E. C. W. de Jong, X. Wang, D. Yang, F. Blaabjerg, V. Cuk, and J. F. G. Cobben, ''The impact of PLL dynamics on the low inertia power grid: A case study of Bonaire Island power system,'' *Energies*, vol. 12, no. 7, p. 1259, 2019.

[12] K. O. H. Pedersen, A. H. Nielsen, and N. K. Poulsen, ''Short-circuit impedance measurement,'' *IEE Proc.-Gener., Transmiss. Distrib.*, vol. 150, no. 2, pp. 169–174, Mar. 2003.

[13] T. Midtsund, J. A. Suul, and T. Undeland, ''Evaluation of current controller performance and stability for voltage source converters connected to a weak grid,'' in *Proc. 2nd Int. Symp. Power Electron. Distrib. Gener. Syst.*, Jun. 2010, pp. 382–388.

[14] A. Etxegarai, P. Eguia, E. Torres, A. Iturregi, and V. Valverde, ''Review of grid connection requirements for generation assets in weak power grids,'' *Renew. Sustain. Energy Rev.*, vol. 41, pp. 1501–1514, Jan. 2015.

[15] E. L. de Aguiar, R. Cardoso, C. M. de Oliveira Stein, J. P. da Costa, and E. G. Carati, ''Distributed renewable power sources in weak grids—Analysis and control,'' in *Renewable Energy-Utilisation and System Integration*. Rijeka, Croatia: InTech, 2016, pp. 199–225.

[16] S. Lu, Z. Xu, L. Xiao, W. Jiang, and X. Bie, ''Evaluation and enhancement of control strategies for VSC stations under weak grid strengths,'' *IEEE Trans. Power Syst.*, vol. 33, no. 2, pp. 1836–1847, Mar. 2018.

[17] S. Harasis and Y. Sozer, ''Improved transient frequency stabilization of grid feeding distributed generation systems using active damping control,'' in *Proc. IEEE Energy Convers. Congr. Expo. (ECCE)*, Sep. 2019, pp. 4324–4330.

[18] Ş. Sönmez and S. Ayasun, ''Gain and phase margins-based delay margin computation of load frequency control systems using Rekasius substitution,'' *Trans. Inst. Meas. Control*, vol. 41, no. 12, pp. 3385–3395, Aug. 2019.

[19] J. Xu, S. Bian, Q. Qian, H. Qian, and S. Xie, ''Robustness improvement of single-phase inverters under weak grid cases by adding grid current feedforward in delay-based phase-locked loop,'' *IEEE Access*, vol. 8, pp. 124275–124287, 2020.

[20] X. Wang, F. Blaabjerg, and W. Wu, ''Modeling and analysis of harmonic stability in an AC power-electronics-based power system,'' *IEEE Trans. Power Electron.*, vol. 29, no. 12, pp. 6421–6432, Dec. 2014.

[21] X. Wang, J. M. Guerrero, F. Blaabjerg, and Z. Chen, ''A review of power electronics based microgrids,'' *Int. J. Power Electron.*, vol. 12, no. 1, pp. 181–192, 2012.

[22] S. Rezaee, A. Radwan, M. Moallem, and J. Wang, ''Voltage source converters connected to very weak grids: Accurate dynamic modeling, small-signal analysis, and stability improvement,'' *IEEE Access*, vol. 8, pp. 201120–201133, 2020.

[23] Z. Miao, H. Tong, W. Yao, and Z. Lu, ''Online measurements of high-band grid impedance using variable frequency carrier based PWM schemes,'' *CSEE J. Power Energy Syst.*, vol. 7, no. 1, pp. 128–139, Jan. 2021.

[24] D. Rebollal, M. Carpintero-Rentería, D. Santos-Martín, and M. Chinchilla, ''Microgrid and distributed energy resources standards and guidelines review: Grid connection and operation technical requirements,'' *Energies*, vol. 14, no. 3, p. 523, Jan. 2021.

[25] M. B. Delghavi, A. Yazdani, and A. Alizadeh, ''Iterative learning control of dispatchable grid-connected distributed energy resources for compensation of grid current harmonic distortions,'' *Int. J. Electr. Power Energy Syst.*, vol. 131, Oct. 2021, Art. no. 107064.

[26] R. Heydari, T. Dragicevic, and F. Blaabjerg, ''High-bandwidth secondary voltage and frequency control of VSC-based AC microgrid,'' *IEEE Trans. Power Electron.*, vol. 34, no. 11, pp. 11320–11331, Nov. 2019.

[27] X. Chen, Y. Zhang, S. Wang, J. Chen, and C. Gong, ''Impedance-phased dynamic control method for grid-connected inverters in a weak grid,'' *IEEE Trans. Power Electron.*, vol. 32, no. 1, pp. 274–283, Jan. 2017.

[28] F. Wang, ''Flexible operation of grid-interfacing converters in distribution networks: Bottom-up solutions to voltage quality enhancement,'' Technische Universiteit Eindhoven, Eindhoven, The Netherlands, Tech. Rep., 2010, pp. 77–101.

[29] S. Albatran, A. Koran, I. A. Smadi, and H. J. Ahmad, ''Optimal design of passive RC-damped LCL filter for grid-connected voltage source inverters,'' *Electr. Eng.*, vol. 100, no. 4, pp. 2499–2508, Dec. 2018.

[30] J. W. Feltes and B. S. Fernandes, ''Wind turbine generator dynamic performance with weak transmission grids,'' in *Proc. IEEE Power Energy Soc. Gen. Meeting*, Jul. 2012, pp. 1–7.

[31] C. Guo, C. Zhao, R. Iravani, H. Ding, and X. Wang, ''Impact of phase-locked loop on small-signal dynamics of the line commutated converter-based high-voltage direct-current station,'' *IET Gener., Transmiss. Distrib.*, vol. 11, no. 5, pp. 1311–1318, 2017.

[32] J. Xu, B. Zhang, Q. Qian, X. Meng, and S. Xie, ''Robust control and design based on impedance-based stability criterion for improving stability and harmonics rejection of inverters in weak grid,'' in *Proc. IEEE Appl. Power Electron. Conf. Exposit. (APEC)*, Mar. 2017, pp. 36s19–3624.

[33] M. Liserre, R. Teodorescu, and F. Blaabjerg, ''Stability of photovoltaic and wind turbine grid-connected inverters for a large set of grid impedance values,'' *IEEE Trans. Power Electron.*, vol. 21, no. 1, pp. 263–272, Jan. 2006.

[34] D. Yang, X. Ruan, and H. Wu, ''Impedance shaping of the grid-connected inverter with LCL filter to improve its adaptability to the weak grid condition,'' *IEEE Trans. Power Electron.*, vol. 29, no. 11, pp. 5795–5805, Nov. 2014.

[35] J. Ni, L. Liu, C. Liu, X. Hu, and A. Li, ''Chaos suppression for a four-dimensional fundamental power system model using adaptive feedback control,'' *Trans. Inst. Meas. Control*, vol. 39, no. 2, pp. 194–207, Feb. 2017.

[36] M. Ramezani, S. Li, and S. Golestan, ''Analysis and controller design for stand-alone VSIs in synchronous reference frame,'' *IET Power Electron.*, vol. 10, no. 9, pp. 1003–1012, Jul. 2017.

[37] Y. Shiohara, T. Tsuji, T. Oyama, T. Shinji, and M. Tadokoro, ''A study on cooperative voltage and frequency control method using distributed generations considering large penetration of renewable energy sources,'' *Electr. Eng. Jpn.*, vol. 197, no. 2, pp. 3–12, Nov. 2016.

[38] S. Yang, Q. Lei, F. Z. Peng, and Z. Qian, ''A robust control scheme for grid-connected voltage-source inverters,'' *IEEE Trans. Ind. Electron.*, vol. 58, no. 1, pp. 202–212, Jan. 2011.

[39] J. Jiao, J. Y. Hung, and R. M. Nelms, ''State feedback control for single-phase grid-connected inverter under weak grid,'' in *Proc. IEEE 26th Int. Symp. Ind. Electron. (ISIE)*, Jun. 2017, pp. 879–885.

SALMAN HARASIS (Member, IEEE) received the B.Sc. degree in electrical power engineering from Tafila Technical University, Tafila, Jordan, in 2009, the M.Sc. degree in electrical engineering from Polytechnic University of Bucharest, Bucharest, Romania, in 2013, and the Ph.D. degree in electrical engineering from The University of Akron, OH, USA, in 2020. He is currently an Assistant Professor with the Department of Electric Power and Mechatronics Engineering, Tafila Technical University. His research interests include control of power systems and microgrids, renewable energy, power electronics, and motor drives for transportation electrification applications.

KARAR MAHMOUD (Member, IEEE) received the B.Sc. and M.Sc. degrees in electrical engineering from Aswan University, Aswan, Egypt, in 2008 and 2012, respectively, and the Ph.D. degree from the Electric Power and Energy System Laboratory (EPESL), Graduate School of Engineering, Hiroshima University, Hiroshima, Japan, in 2016. Since 2010, he has been with Aswan University, where he is currently an Associate Professor with the Department of Electrical Engineering, Faculty of Engineering. He is also a Postdoctoral Researcher with Prof. M. Lehtonen's Group at the School of Electrical Engineering, Aalto University, Finland. He has authored or coauthored several publications in top-ranked journals, including IEEE journals, international conferences, and book chapters. His research interests include power systems, renewable energy sources, smart grids, distributed generation, optimization, applied machine learning, the IoT, industry 4.0, and electric vehicles. Since 2021, he becomes a Topic Editor in *Sensors* and *Energies* (MDPI) journals, and is a Guest Editor for two special issues in *Catalysts* and *Forecasting* (MDPI) journals.

SAHER ALBATRAN (Senior Member, IEEE) received the B.Sc. degree in electric power engineering from Yarmouk University, Irbid, Jordan, in 2005, the M.Sc. degree in electric power and control engineering from Jordan University of Science and Technology, Irbid, in 2008, and the Ph.D. degree in electrical engineering from Mississippi State University, Mississippi State, MS, USA, in 2013. He is currently the Vice Dean of research and an Associate Professor with Jordan University of Science and Technology. His research interests include control of power electronics, pulsewidth modulation, inverter topologies, power system operation, renewable energy, and filter design and control.

KHALED ALZAAREER (Member, IEEE) received the Ph.D. degree in electrical engineering from the École de Technologie Supérieure, Montreal, Canada, in 2020. His main research interests include control, modeling, grid integration of renewable energy systems, power control and energy management microgrids, islanding detection schemes, and development of power flow algorithms in AC microgrids, including optimization and control of DG power converters.

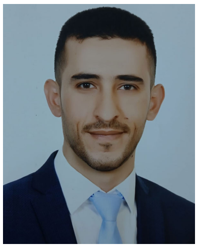

QUSAY SALEM (Member, IEEE) received the Ph.D. degree in electrical power and energy engineering from Ulm University, Germany, in February 2020. His Ph.D. study were fully funded by the Deutscher Akademischer Austausch Dienst (DAAD) as he has been shortlisted and awarded the DAAD Ph.D. scholarship. Since September 2020, he has been serving as an Assistant Professor for the Department of Electrical Engineering, Princess Sumaya University for Technology (PSUT). His doctoral work has mainly focused on the bidirectional power flow control in low-voltage AC microgrids by implementing novel and sophisticated control and optimization techniques. His research interests include decentralized power control and energy management in low-voltage smart microgrids, islanding detection schemes, and development of power flow algorithms in AC microgrids, including optimization, control of DG power converters, and application of FACTS devices in power systems.